Comparison of full scale and wind tunnel measurements of the spatial distribution of turbulence components over the Bolund Island

Cuerva-Tejero, A., Gallego-Castillo, C., Lopez-Garcia, O., Perez-Alvarez, J., Yeow, T.S.

13th May 2015

Universidad Politénica de Madrid

1   Introduction

We present experimental spatial distributions of turbulence intensity components over a 1:115 scale model of the Bolund hill. Our measurements are determined in a boundary layer wind tunnel (WT) without stratification. Our results are compared with full scale (FS) ones. The FS results are obtained from the analysis of the database provided by RISØ-DTU after the Bolund experiment. This experiment was conducted by them during a 3-month period in the winter of 2007-2008 [1]. Three component time resolved hotwire anemometry (3CHW) and two component particle image velocimetry (PIV) are used in our experiment.

Bolund is a hill of about 130 m×75 m×12 m, surrounded by water with a long uniform fetch for most of the upstream directions of interest. The Bolund experiment is probably the most relevant test case of flow models oriented to wind energy analysis, in this case, over highly complex terrains, in neutral conditions and non affected by Coriolis forces. The mentioned FS conditions make the Bolund test an ideal case for wind tunnel modeling. Several numerical and physical models have been applied during the Bolund experiment and also after it [1, 2, 3, 7, 9].

One of the main geometric characteristics of Bolund is the escarpment facing westerly winds (see figure 1). For westerly winds, the geometry of Bolund guarantees that flow detaches at the edge, provided a sufficiently large Reynolds number. The long (in the mean flow direction) flat top ensures reattachment of the flow on the island. For this direction, the lee side of the hill presents a slope with a maximum inclination around -40°, leading as well to intermittent recirculation patterns. The existence of detachment at the escarpment has been verified by full-scale measurements of intermittent recirculation patterns downstream of the escarpment edge (see [6] and figure 13 in [3]). Intermittent recirculation patterns have been also visualized by means of PIV in wind tunnel, for the 270° wind direction,[8], [9].

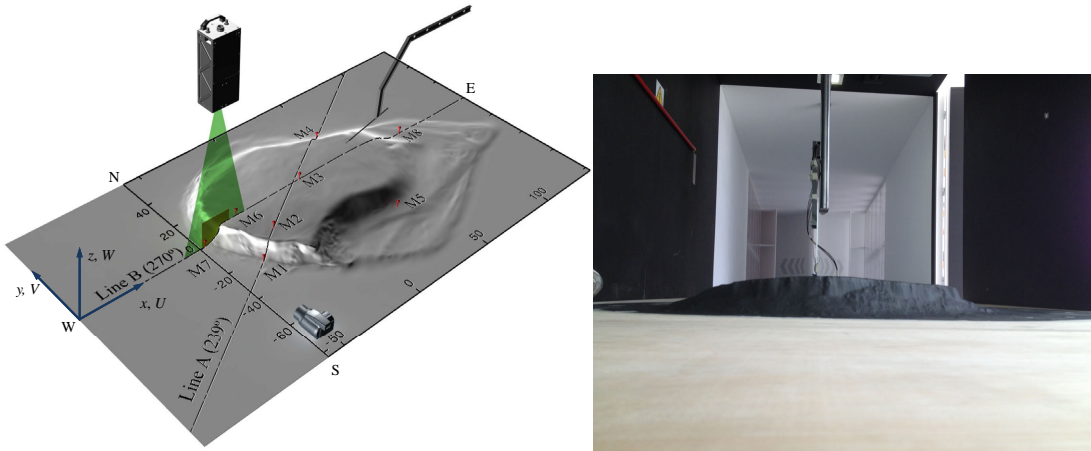Most of the published results are focused on the values of mean speed and turbulent kinetic energy

Figure 1: Mounting of the 3CHW probe 55P91 and its support, see [5]. $[x, y, z]$ is the Bolund reference system.

at the locations where the met mast were installed in the FS experiment. Our interest is now in how the turbulent kinetic energy is distributed among the velocity components (what is relevant for wind turbine response), and to which extent our wind tunnel experiment can reproduce these distributions. Aimed to put some light on these questions, we have calculated metrics of the bias of the WT results respect to the FS ones. We have established if there is some kind of dependency between the bias the two velocimetry techniques employed or related to the test Reynolds number.

2 Approach

Since we are specially concerned in how the turbulent kinetic energy (TKE) is distributed among the velocity components, the accuracy in the determination of the different components of the instantaneous velocity is a must for us. This is why we have extremely cared the positioning and orientation of the sensors (3CHW probe, PIV camera and laser head) and the calibration process (see figure 2). With this regard, we have developed a new directional calibration algorithm for 3CHW probes which leads to a higher directional accuracy. In figure 3 we present results for the inclination flow angle versus the direction flow angle determined by the 3CHW probe during one of our calibration tests. The results obtained after applying the standard calibration algorithm (Measured RMS, root mean squared) and the new one (Measured Directional) are compared with the true value (Geometric).
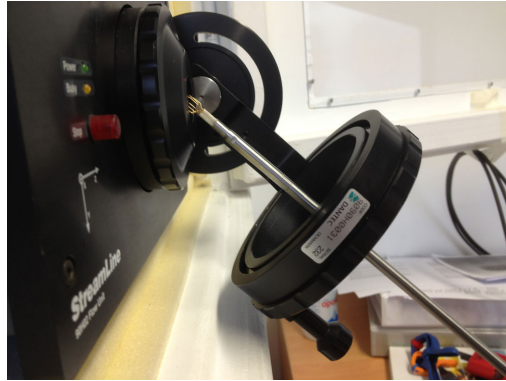
Figure 2: The used 3CHW probe DANTEC 55P91 during a directional calibration test in our ACLA16 WT.
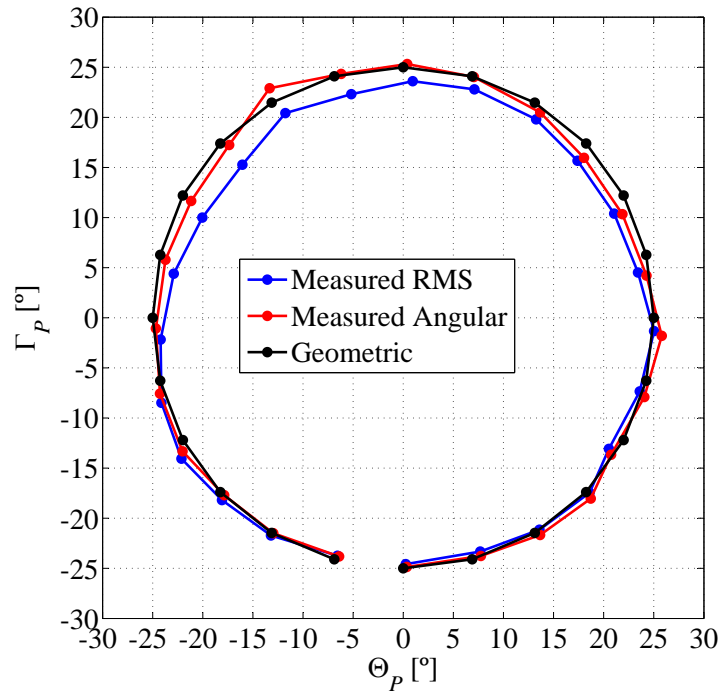

Figure 3: Inclination angle Γ_P versus direction angle Θ_P reproduced during a directional calibration test.

	Full-scale	Re_{h1}			Re_{h2}		
		2CHW	3CHW	PIV	2CHW	3CHW	PIV
δ [m]	-	0.240	0.220	-	0.230	0.210	-
u_* [m/s]	-	0.314	0.293	0.306	0.596	0.572	0.565
u_{*05} [m/s]	0.47	0.270	0.267	0.247	0.497	0.520	0.484
$z_0 \times 10^5$ [m]	60	1.04	1.08	1.02	0.52	0.54	0.59
$\hat{\theta} \times 10^3$ [m]	-	20.0	20.3	-	18.4	18.1	-
$h^{-1}\delta$	-	2.343	2.148	-	2.245	2.050	-
$I_u\|_{h_0} \times 10^2$	12.0	9.3	10.0	9.5	8.6	9.2	9.4
$I_v\|_{h_0} \times 10^2$	8.0	-	7.1	-	-	6.6	-
$I_w\|_{h_0} \times 10^2$	5.0	5.1	5.5	4.9	4.9	5.1	4.7
$I_u\|_h \times 10^2$	-	0.073	0.075	0.073	0.064	0.068	0.074
$I_v\|_h \times 10^2$	-	-	5.4	-	-	5.0	-
$I_w\|_h \times 10^2$	-	4.1	4.3	4.3	3.9	4.0	3.9
$\sigma_v/\sigma_u\|_{h_0}$	0.76	-	0.70	-	-	0.71	-
$\sigma_w/\sigma_u\|_{h_0}$	0.46	-	0.54	0.52	-	0.55	0.51
$h^{-1}L_u^x$	-	-	3	-	-	3.5	-
$U_\delta\hat{\theta}\nu^{-1} \times 10^{-4}$	-	1.04	1.00	-	1.92	1.80	-
$u_*z_0\nu^{-1}$	18	0.219	0.212	0.208	0.206	0.205	0.226
$\mathrm{Je} = h\,z_0^{-1} \times 10^{-4}$	1.96	0.98	0.94	1.00	1.97	1.90	1.70

Table 1: Main characteristics of the undisturbed inflow boundary layer for $\mathrm{Re}_{h1} = 4.15 \times 10^4$ and $\mathrm{Re}_{h2} = 8.21 \times 10^4$. The lengths δ and z_0 for the wind tunnel simulations are shown in WT scale. The declared interval for the FS Reynolds number is $4.25 \times 10^6 \leqslant \mathrm{Re}_h \leqslant 10.2 \times 10^6$. A reference value for the boundary layer height $\delta = 0.22\,\mathrm{m}$ is selected hereafter. $\hat{\theta}$ is the momentum thickness.

3   Main results

The flow field in the empty test section of our WT has been measured using three techiques (PIV, 2CHW and 3CHW) to have redundancy measurements in order to cross check the quality of the results. The velocity profiles from the empty WT were used as reference inflow conditions. Reference measurements were taken at the two test Reynolds numbers based in the maximum height of the island, h, and the upstream speed at this height, U_h, $\mathrm{Re}_{h1} = 4.15 \times 10^4$ and $\mathrm{Re}_{h2} = 8.21 \times 10^4$. The main characteristics of the inflow boundary layer are presented in table 1 and in figure 4.

We analyze the flow field for a 270° wind direction and we present results along transects at two heights (2 m and 5 m a.g.l) along line B in the Bolund community jargon, see figure 5.

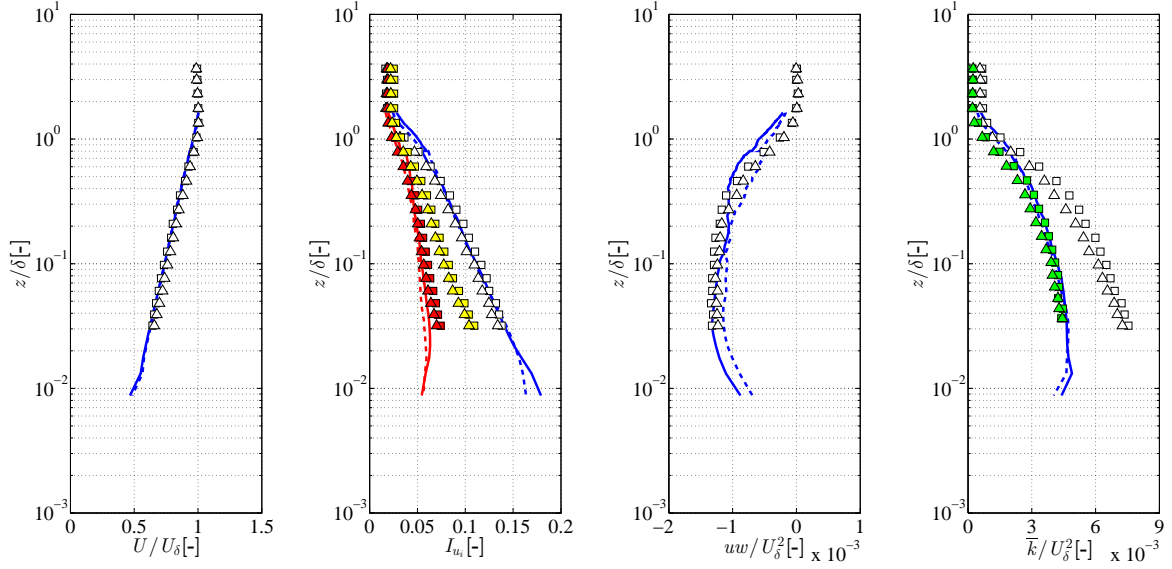In figures 6, 7 and 8 we present the value of the longitudinal, lateral and vertical turbulence intensities,

Figure 4: Basic statistics of the ACLA16 WT boundary layer with the lay-out used in the tests. Continuous lines: PIV for Re_{h1}, dashed lines: PIV for Re_{h2}, squares: 3CHW for Re_{h1} and triangles: 3CHW for Re_{h2}. In the second graph, white symbols: u, yellow symbols: v, and red symbols: w. In the rightmost graph, the green symbols represent the "two-components" TKE, $\bar{k}_{2\mathrm{C}}$ calculated from the 3CHW measurements.
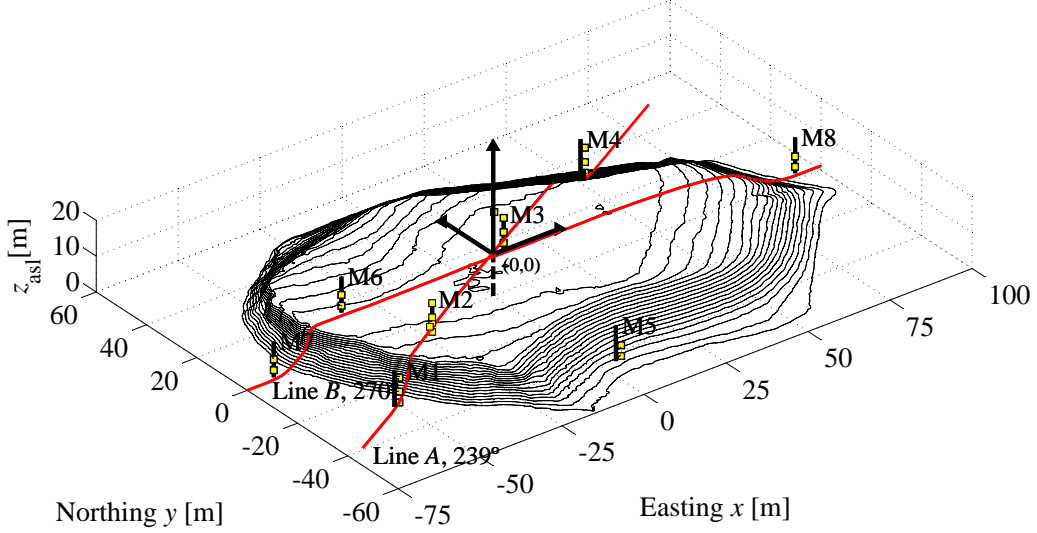
Figure 5: Met masts locations in the Bolund experiment. The reference met mast M0 is located in coordinates $[-181.1\,\mathrm{m}, -101.7\,\mathrm{m}]$ not shown in the figure. Ultrasonic anemometers: yellow squares. The Bolund reference system is indicated in the figure. From [4].

respectively. The results are normalized with the corresponding value at the reference upstream location. The results are presented for transects at 2 m and 5 m height a.g.l, the two mentioned test Reynolds numbers and for the 3CHW and PIV techniques. The full scale results are also indicated for comparison purposes.

In figures 9 and 10 we present the value of the ratios of the standard deviations the velocity component fluctuations. In the case of the normalized turbulence intensity, I_v/I_{v05}, and the ratio, σ_v/σ_u, no-results for PIV are presented since our PIV technique is not stereo PIV, and the v component of the flow velocity is not resolved.

In tables 2 and 3 we present the bias of our WT results related to the FS results at the met mast locations, according to the expression

$$\epsilon_{I_{u_i}} = 100\frac{I_{u_i}I_{u_i05}^{-1}\big|_{WT} - I_{u_i}I_{u_i05}^{-1}\big|_{FS}}{\left|I_{u_i}I_{u_i05}^{-1}\right|_{FS}},$$

for the normalized turbulence intensities, and

$$\epsilon_{\sigma_{u_i}\sigma_u^{-1}} = 100\frac{\sigma_{u_i}\sigma_u^{-1}\big|_{WT} - \sigma_{u_i}\sigma_u^{-1}\big|_{FS}}{\left|\sigma_{u_i}\sigma_u^{-1}\right|_{FS}},$$

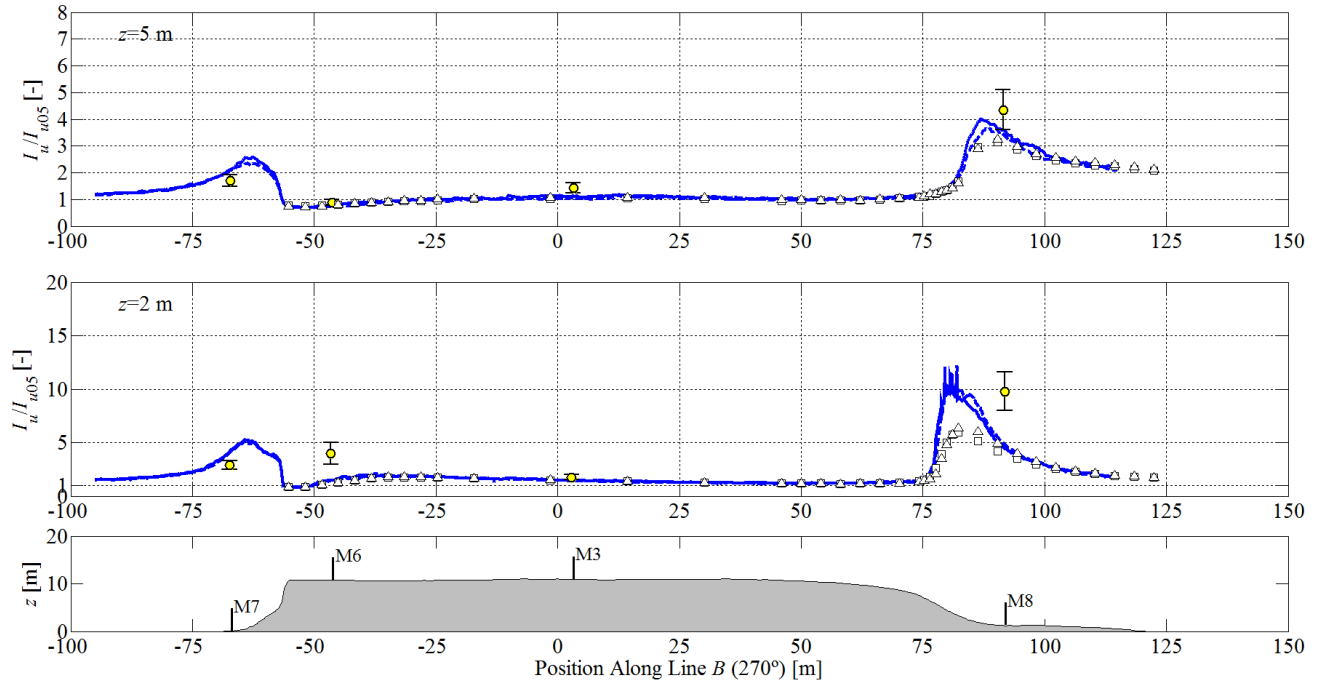for the ratios of the standard deviations of flow velocity fluctuations.

6

Figure 6: Normalized longitudinal turbulence intensity I_u/I_{u05} at $z = 2\,\mathrm{m}$ a.g.l. and $z = 5\,\mathrm{m}$ a.g.l.: Continuous lines, PIV for Re_{h1}; dashed lines, PIV for Re_{h2}; squares, 3CHW for Re_{h1}; triangles, 3CHW for Re_{h2}. Full-scale results (yellow dots with uncertainty bars). Velocity components expressed in the wind reference system. Line B. Wind direction 270°.

Figure 7: Normalized lateral turbulence intensity I_v/I_{v05} at $z = 2\,\mathrm{m}$ a.g.l. and $z = 5\,\mathrm{m}$ a.g.l.: Squares, 3CHW for Re_{h1}; triangles, 3CHW for Re_{h2}. Full-scale results (yellow dots with uncertainty bars). Velocity components expressed in Bolund reference system. Line B. Wind direction $270°$.
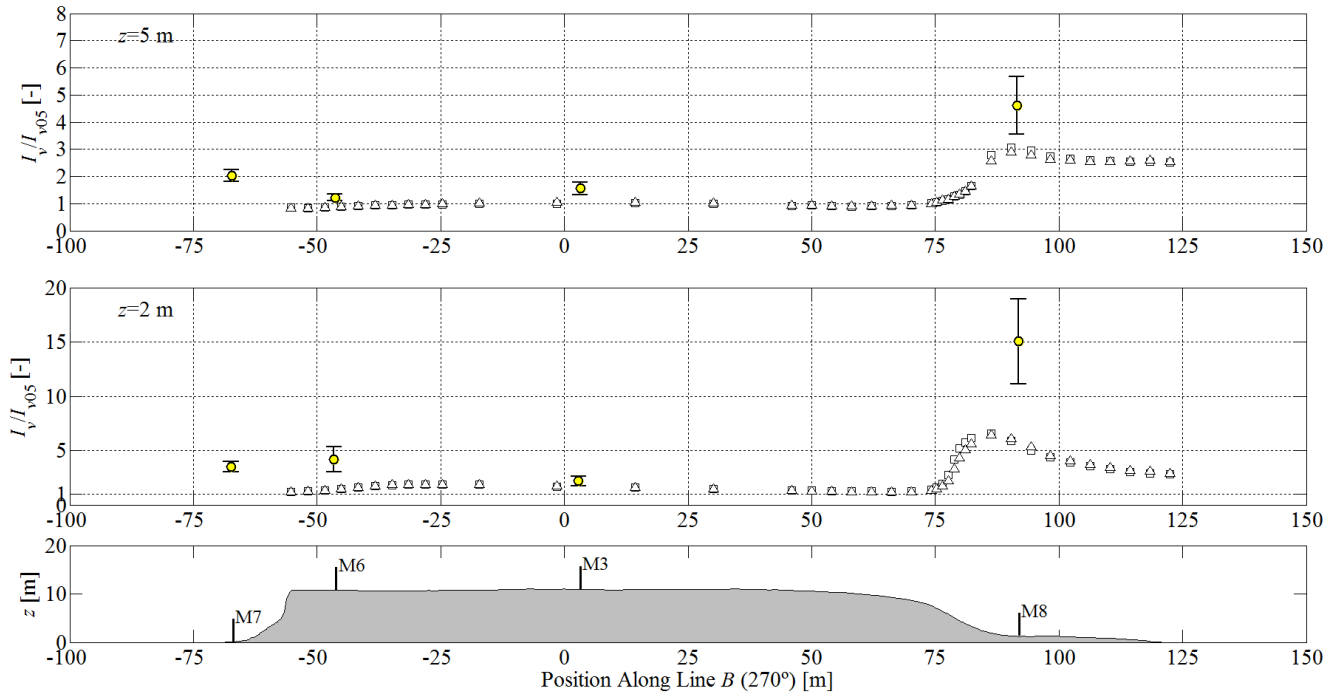
Figure 8: Normalized vertical turbulence intensity I_w/I_{w05} at $z = 2\,\mathrm{m}$ a.g.l. and $z = 5\,\mathrm{m}$ a.g.l.: Continuous lines, PIV for Re_{h1}; dashed lines, PIV for Re_{h2}; squares, 3CHW for Re_{h1}; triangles, 3CHW for Re_{h2}. Full-scale results (yellow dots with uncertainty bars). Velocity components expressed in Bolund reference system. Line B. Wind direction $270°$.
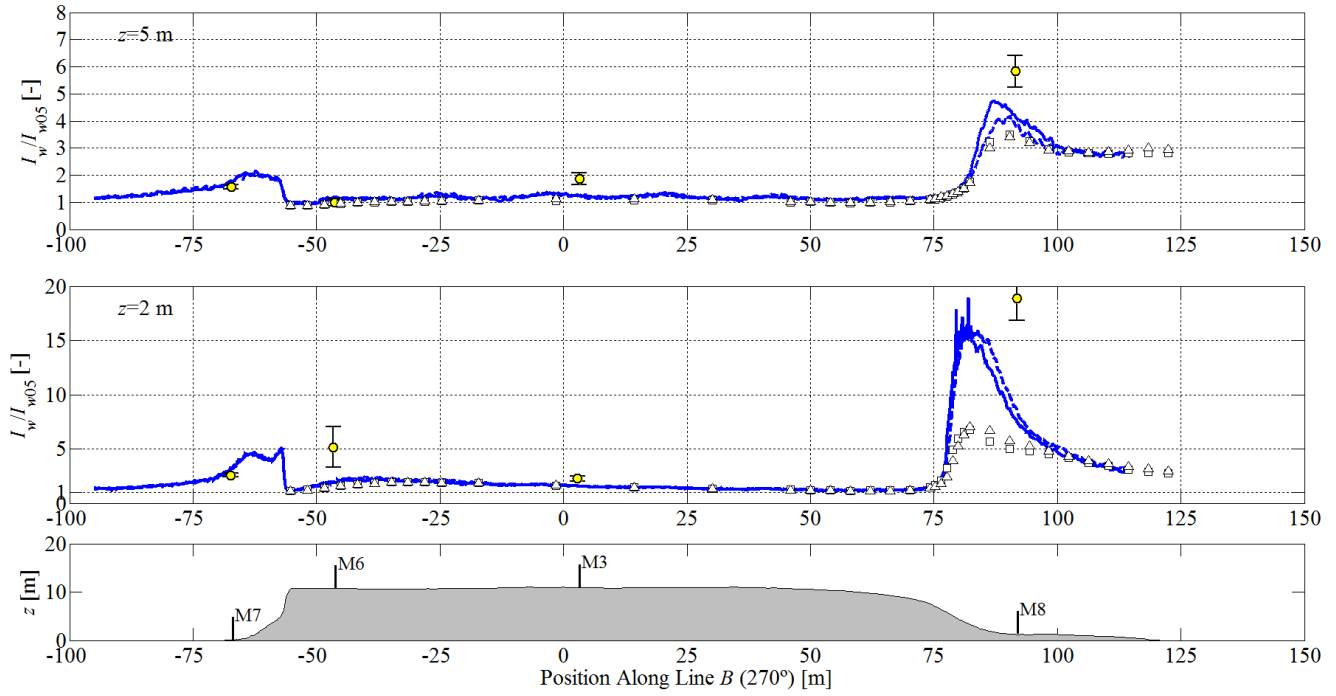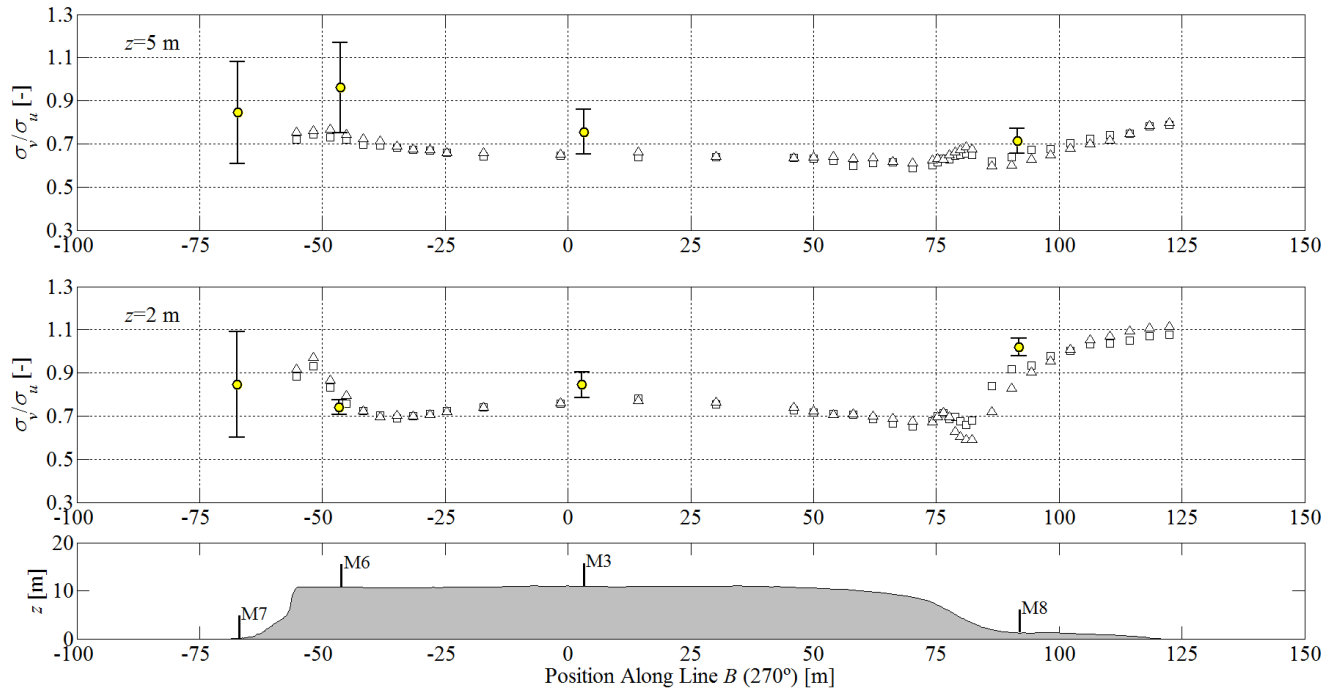
Figure 9: Ratio of standard deviations σ_v/σ_u on a isoheight line at $z = 2\,\mathrm{m}$ a.g.l. and $z = 5\,\mathrm{m}$ a.g.l.. Squares: 3CHW for Re_{h1} and triangles: 3CHW for Re_{h2}. Full-scale results (yellow dots with uncertainty bars). Line B. Wind direction 270°.

Figure 10: Ratio of standard deviations σ_w/σ_u on a isoheight line at $z = 2\,\mathrm{m}$ a.g.l. and $z = 5\,\mathrm{m}$ a.g.l.. Continuous lines: PIV for Re_{h1}, dashed lines: PIV for Re_{h2}, squares: 3CHW for Re_{h1} and triangles: 3CHW for Re_{h2}. Full-scale results (yellow dots with uncertainty bars). Line B. Wind direction $270°$.
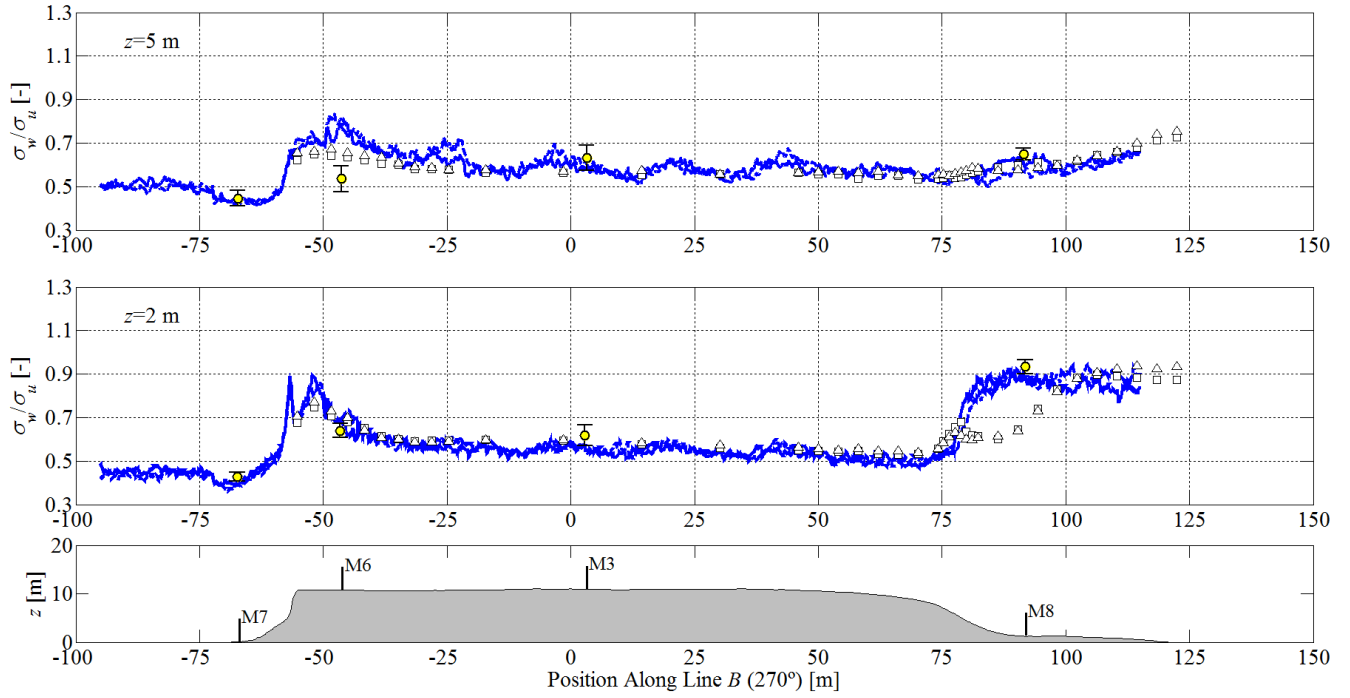
%	M7	M6	M3	M8	MAE	MAE*
ϵ_{I_u}	40.8	-67.3 (W)	-17.6 (B)	-54.4	45.1	46.5
ϵ_{I_v}		-66.1 (W)	-23.4 (B)	-62.4	-	50.6
ϵ_{I_w}	21.8 (B)	-66.9 (W)	-29.7	-64.7	45.8	53.7
$\epsilon_{\sigma_w \sigma_u^{-1}}$	-8.1	8.4	-6.2 (B)	-16.1 (W)	9.7	10.3
$\epsilon_{\sigma_v \sigma_u^{-1}}$	-	9.2 (B)	-9.7	-12.6 (W)	-	10.5
$\epsilon_{\Delta S}$	-1.5 (B)	52.9 (W)	14.0	18.1	21.6	28.3
$\epsilon_{\Delta \overline{k}}$	12.2 (B)	-190.1 (W)	-34.6	-39.3	69.0	88.0

Table 2: Bias in the determination of turbulence intensities, ratios of standard deviations, speed-up and normalized increase of TKE. $z = 2\,\mathrm{m}$. MAE indicates the absolute mean bias from M7, M6, M3 and M8, and MAE* from M6, M3 and M8. $\epsilon_{\Delta S}$ and $\epsilon_{\Delta \overline{k}}$ have been reproduced from [9]. (W) worst predicted, (B) best predicted.

%	M7	M6	M3	M8	MAE	MAE*
ϵ_{I_u}	23.3	-13.2 (B)	-25.1 (W)	-23.8	21.4	20.7
ϵ_{I_v}		-28.6 (B)	-34.2	-36.1 (W)	-	33.0
ϵ_{I_w}	12.9	6.8 (B)	-37.4 (W)	-36.5	23.4	26.9
$\epsilon_{\sigma_w \sigma_u^{-1}}$	-2.7 (B)	35.2 (W)	-8.4	-9.1	13.8	17.6
$\epsilon_{\sigma_v \sigma_u^{-1}}$		-23.2 (W)	-14.1	-12.0 (B)	-	16.4
$\epsilon_{\Delta S}$	1.7 (B)	-6.1	11.3	16.0 (W)	8.8	11.1
$\epsilon_{\Delta \overline{k}}$	11.7 (B)	-29.8	-43.3 (W)	-34.6	29.8	35.9

Table 3: Bias in the determination of turbulence intensities, ratios of standard deviations, speed-up and normalized increase of TKE. $z = 5\,\mathrm{m}$. MAE indicates the absolute mean bias from M7, M6, M3 and M8, and MAE* from M6, M3 and M8. $\epsilon_{\Delta S}$ and $\epsilon_{\Delta \overline{k}}$ have been reproduced from [9]. (W) worst predicted, (B) best predicted.

4 Conclusions

Our new directional calibration algorithm improves the precision of the 3CHW measurements. No significant differences are found between results for different Reynolds numbers and different experimental techniques.

The bias results show that, for the normalized turbulence intensities, the bias are higher (as expected) for $z = 2\,\mathrm{m}$ than for $z = 5\,\mathrm{m}$, ranging from the largest bias (-66.9%) for I_w/I_{w05} in M6 at $z = 2\,\mathrm{m}$ to the lowest bias (6.8%) for I_w/I_{w05} in M6 at $z = 5\,\mathrm{m}$. The predictions of the ratios $\sigma_{u_i}\sigma_u^{-1}$ are rather good and this means that the fluctuation energy of one flow velocity component relative to another is well captured.

5   Learning objectives

To show that traditional directional calibration techniques of 3CHW can be improved.

To contribute to quantify which precision can be achieved in the determination of turbulence intensities of flow velocity components in a wind tunnel test of a complex terrain.

To contribute to quantify the influence of Reynolds number and experimental techniques in the determination of turbulence intensities in a wind tunnel test of a complex terrain.

References

[1] A. Bechmann, J. Berg, M. S. Courtney, J. Jørgensen, H.E. Mann, and N. N. Sørensen. The Bolund Experiment: Overview and Background. Technical Report Risø-R-1658(EN), Risø, 2009.

[2] A. Bechmann, N. N. Sørensen, J. Berg, J. Mann, and P. E. Rethore. The Bolund Experiment, Part II: Blind Comparison of Microscale Flow Models. *Boundary-Layer Meteorology*, 141(2):219–243, 2011.

[3] J. Berg, J. Mann, A. Bechmann, M. S. Courtney, and H. E. Jørgensen. The Bolund Experiment, Part I: Flow Over a Steep, Three-Dimensional Hill. *Boundary-Layer Meteorology*, 141(2):219–243, 2011.

[4] A. Cuerva, T.S. Yeow, C. Gallego-Castillo, and O. López-García. Effects of the water level on the flow topology over the Bolund island. In *J. Phys.: Conf. Ser.*, number 514. IOPScience, 2014.

[5] F. E. Jørgensen. How to measure turbulence with hot-wire anemometers-a practical guide. Technical report, DANTEC Dynamics, 2002.

[6] J. Mann, N. Angelou, T. Mikkelsen, K. H. Hansen, D. Cavar, and J. Berg. Laser Scanning of a Recirculation Zone on the Bolund Escarpment. In *The Science of Making Torque from Wind, October, 9-11, Oldenburg*, 2012.

[7] J. M. Prospathopoulos, E. S. Politis, and P. K. Chaviaropoulos. Application of a 3D Rans Solver on the Complex Hill of Bolund and Assessment of the Wind Flow Predictions. *Journal of Wind Engineering and Industrial Aerodynamics*, 107:149–159, 2012.

[8] T. S. Yeow, A. Cuerva, B. Conan, and J. Pérez. Wind Tunnel Analysis of the Detachment Bubble on Bolund Island. In *The Science of Making Torque from Wind, October, 9-11, Oldenburg*, 2012.

[9] T. S. Yeow, A. Cuerva, and J. Pérez-Alvarez. Reproducing the Bolund experiment in wind tunnel. *Wind Energy*, 18(1):153–169, 2015.